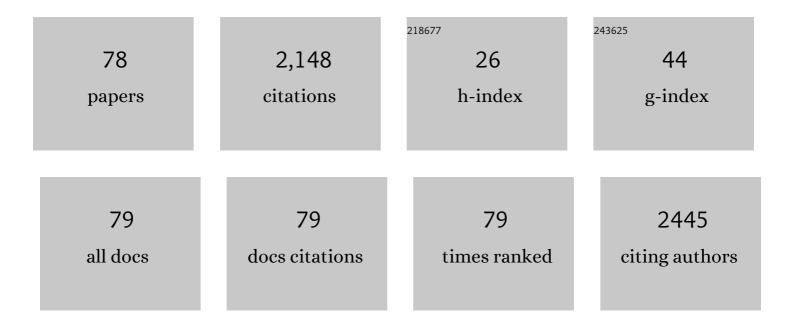
Yuxuan Xie

List of Publications by Year in descending order

Source: https://exaly.com/author-pdf/1761088/publications.pdf Version: 2024-02-01



VIIVIIAN XIE

1 Formation of Magnesium Dendrites during Electrodeposition. ACS Energy Letters, 2019, 4, 375-376. 2 Microstructural evolution of pure magnesium under high strain rate loading. Acta Materialia, 2015, 87, 56-67. 3 Pyramidal I slip in cases compressed Mg single crystals. Scripta Materialia, 2016, 112, 75-78. 4 Strengthening from Nb-rich clusters in a Nb-microalloyed steel. Scripta Materialia, 2017, 136, 202-214. 6 Microstructural characterization of boren-rich boron carbide. Acta Materialia, 2017, 136, 202-214. 7 Magning mechanisms and growth regimes of magnesium electrodeposition at high current denatities. 8 Anomolous work bracking behavior of Fe40Mr 400Ci IOCol 0 high entropy alloy single crystals 9 Bioactive mesoporesEcplass microspheres with controllable protein564elwery properties by biomimetic aurface modification. Journal of Biomedical Materialis Research. Part A, 2010, 95A, 476-485. 10 Narotwinned metal MEMS films with unprecedented strength and stability. Science Advances, 2017, 3, e1700685. 11 Superstrength through Nanotwinning. Nano Letters, 2016, 16, 7573.7579. 12 Atterials. Science Xamp JE formedical and Jiac Wilk Materials. Properties. Microstineture and Processing, 2100, 252, 415-418. 13 New Ground-State Crystal Structure of Elemental Boron. Physical Review Letters, 2016, 117, 085501. 14 Enter of NM Increality and Naterinalis. Propereties. Microstrucure and Processing, 210, 2	IF	CITATIONS
 87, 56-67. Pyramidal I slip in classis compressed Mg single crystals. Scripta Materialia, 2016, 112, 75-78. Strengthening from Nb-rich clusters in a Nb-microalloyed steel. Scripta Materialia, 2012, 66, 710-713. Microstructural characterization of boron-rich boron carbide. Acta Materialia, 2017, 136, 202-214. Nanocrystalline F-Ti alloy with high hardness, low Young's modulus and excellent in vitro biocompatibility for biomedical applications. Mow Young's modulus and excellent in vitro biocompatibility for biomedical applications. Mow Young's modulus and excellent in vitro biocompatibility for biomedical applications. Mow Young's modulus and excellent in vitro biocompatibility for biomedical applications. Mow Young's modulus and excellent in vitro biocompatibility for biomedical applications. Mow Young's modulus and excellent in vitro biocompatibility of biomedical applications. Mow Young's modulus and excellent in vitro Materials Horizons, 2020, 7, 843-854. Anomalous work hardening behavior of Fe40Mn40Cr10Co10 bigh entropy alloy single crystals deformed by twinning and silp. Acta Materials, 2019, 181, 555-569. Bioactive mesoporeaSeglass microspheres with controllable protein&cfellwery properties by biomimetic surface modification. Journal of Biomedical Materials Research - Part A, 2010, 95A, 476-485. Nanotwinned metal MEMS films with unprecedented strength and stability. Science Advances, 2017, 3, e1700685. Superstrength through Nanotwinning. Nano Letters, 2016, 16, 7573-7579. New Ground-State Crystal Structure of Elemental Boron. Physical Review Letters, 2016, 117, 085501. New Ground-State Crystal Structure of Elemental Boron. Physical Review Letters, 2016, 117, 085501. Inhanced grain refinement of an Al&C''Mg&G'' alloy by high-pressure torsion processing at 100A^oC. Materials Science X ampt Engineering A' Structural Materials. Properties, Microstructure an	17.4	221
 Strengthening from Nb-rich clusters in a Nb-microalloyed steel. Scripta Materialia, 2012, 66, 710-713. Microstructural characterization of boron-rich boron carbide. Acta Materialia, 2017, 136, 202-214. Nanocrystalline ¹²-Ti alloy with high hardness, low Young's modulus and excellent in vitro biocompatibility for biomedical applications. Materials Science and Engineering C, 2013, 33, 3530-3536. Mapping mechanisms and growth regimes of magnesium electrodeposition at high current densities. Materials Horizons, 2020, 7, 843-854. Anomalous work hardening behavior of Fe4OMn40Cr10Co10 high entropy alloy single crystals deformed by twinning and slip. Acta Materialia, 2019, 181, 555-569. Bloactive mesopore&Eglass microspheres with controllable protein&Eddelivery properties by biomimetic surface modification. Journal of Biomedical Materials Research - Part A, 2010, 95A, 476-485. Nanotwinned metal MEMS films with unprecedented strength and stability. Science Advances, 2017, 3, e1700685. Superstrength through Nanotwinning. Nano Letters, 2016, 16, 7573-7579. Atomic-Level Understanding of &EccAsymmetric Twins&Erin Boron Carbide. Physical Review Letters, 2015, 115, 175501. New Ground-State Crystal Structure of Elemental Boron. Physical Review Letters, 2016, 117,085501. Enhanced grain refinement of an Al&C'Mg&C'Si alloy by high-pressure torsion processing at 100A°C. Materials Science & amp; Engineering & Structurel and Properties, Microstructure and Processing, 2012, 523, 415-418. Effect of Nb Microalloying and Hot Rolling on Microstructure and Properties of Ultrathin Cast Strip Steels. Produced by the CASTRIPA® Process. Metallurgical and Materials Transactions A: Physical Metarials Science, 2011, 42, 2199-2206. Locating Si atoms in Skdoped boron carbide: A route to understand amorphization mitigation mechanism. Acta Materiala, 2018, 157, 106-113. <l< td=""><td>7.9</td><td>168</td></l<>	7.9	168
Microstructural characterization of boron-rich boron carbide. Acta Materialia, 2017, 136, 202-214. Nanocrystalline [2-Ti alloy with high hardness, low Young's modulus and excellent in vitro biocompatibility for biomedical applications. Materials Science and Engineering C, 2013, 33, 3530-3536. Mapping mechanisms and growth regimes of magnesium electrodeposition at high current densities. Materials Horizons, 2020, 7, 843-854. Anomalous work hardening behavior of Fe40Mn40Cr10Co10 high entropy alloy single crystals deformed by twinning and slip. Acta Materialia, 2019, 181, 555-569. Bloactive mesopore&Eglass microspheres with controllable protein&Cdelivery properties by blominnetic surface modification. Journal of Biomedical Materials Research - Part A, 2010, 95A, 476-485. Nanotwinned metal MEMS films with unprecedented strength and stability. Science Advances, 2017, 3, e1700685. New Ground-State Crystal Structure of Elemental Boron. Physical Review Letters, 2016, 117, 085501. New Ground-State Crystal Structure of Elemental Boron. Physical Review Letters, 2016, 117, 085501. Enhanced grain refinement of an Al&E ^M Mg&C ^M Si alloy by high-pressure torsion processing at 100Å ^o C. Microstructure and Processing and Hoc Poncess. Metallingted and Materials: Properties of Ultrathin Cast Strip Structure IM Controlley Process and Properties of Ultrathin Cast Strip Street by Process Metallingted and Materials: Properties of Ultrathin Cast Strip Street By Process Metallingted and Materials Transactions A: Physical Metallingted and Materials Tran	5.2	105
 Nanocrystalline ¹²-Ti alloy with high hardness, low Young's modulus and excellent in vitro biocompatibility for biomedical applications. Materials Science and Engineering C, 2013, 33, 3530-3536. Mapping mechanisms and growth regimes of magnesium electrodeposition at high current densities. Materials Horizons, 2020, 7, 843-854. Anomalous work hardening behavior of Fe40Mn40Cr10Co10 high entropy alloy single crystals deformed by twinning and slip. Acta Materialia, 2019, 181, 555-569. Bioactive mesopore&Eglass microspheres with controllable protein&Edelivery properties by biomimetic surface modification. Journal of Biomedical Materials Research - Part A, 2010, 95A, 476-485. Nanotwinned metal MEMS films with unprecedented strength and stability. Science Advances, 2017, 3, e1700685. Superstrength through Nanotwinning. Nano Letters, 2016, 16, 7573-7579. Atomic-Level Understanding of &EœAsymmetric Twins&Evin Boron Carbide. Physical Review Letters, 2015, 115, 175501. New Ground-State Crystal Structure of Elemental Boron. Physical Review Letters, 2016, 117, 085501. Erhanced grain refinement of an Al&E''Mg&C'Si alloy by high-pressure torsion processing at 100ŰC. Materials Science & Amp; Engineering A: Structural Materials: Properties of Ultrathin Cast Strip Processing, 2012, 552, 415-418. Effect of Nb Microalloying and Hot Rolling on Microstructure and Properties of Ultrathin Cast Strip Metallurgy and Materials Science, 2011, 42, 2199-2206. Locating Si atoms in Si-doped boron carbide: A route to understand amorphization mitigation mechanism. Acta Materialia, 2018, 157, 106-113. Significant disparity of non-basal dislocation activities in hot-rolled highly textured Mg and Mg-3A-12n alloy under tension. Acta Materialia, 2021, 207, 116691. Effect of Alumina on the Structure and Mechanical Properties of Spark Plasma Sintered Boron 	5.2	91
 biocompatibility for biomedical applications. Materials Science and Engineering C, 2013, 33, 3530-3536. Mapping mechanisms and growth regimes of magnesium electrodeposition at high current densities. Materials Horizons, 2020, 7, 843-854. Anomalous work hardening behavior of Fe40Mn40Cr10Co10 high entropy alloy single crystals deformed by twinning and slip. Acta Materialia, 2019, 181, 555-569. Bioactive mesopore&glass microspheres with controllable protein&edelivery properties by biomimetic surface modification. Journal of Biomedical Materials Research - Part A, 2010, 95A, 476-485. Nanotwinned metal MEMS films with unprecedented strength and stability. Science Advances, 2017, 3, e1700685. Superstrength through Nanotwinning. Nano Letters, 2016, 16, 7573-7579. Atomic-Level Understanding of &cœAsymmetric Twins&Ein Boron Carbide. Physical Review Letters, 2015, 115, 175501. New Cround-State Crystal Structure of Elemental Boron. Physical Review Letters, 2016, 117, 085501. Enhanced grain refinement of an Al&C*Mg&C*Si alloy by high-pressure torsion processing at 100Å*C. Materials Science & amp; Engineering A: Structural Materials: Properties, Microstructure and Processing, 2012, 552, 415-418. Ffect of Nb Microalloying and Hot Rolling on Microstructure and Properties of Ultrathin Cast Strip Steles Produced by the CASTRIPA * Process. Metallurgical and Materials Transactions A: Physical Metallurgy and Materials, 2018, 157, 106-113. Significant disparity of non-basal dislocation activities in hot-rolled highly-textured Mg and Mg*Al-IZn alloy under tension. Acta Materialia, 2012, 202, 116691. Effect of Alumina on the Structure and Mechanical Properties of Spark Plasma Sintered Boron 	7.9	91
 Materials Horizons, 2020, 7, 843-854. Anomalous work hardening behavior of Fe40Mn40Cr10Co10 high entropy alloy single crystals deformed by twinning and slip. Acta Materialia, 2019, 181, 555-569. Bioactive mesopore@cglass microspheres with controllable protein@cdelivery properties by biomimetic surface modification. Journal of Biomedical Materials Research - Part A, 2010, 95A, 476-485. Nanotwinned metal MEMS films with unprecedented strength and stability. Science Advances, 2017, 3, e1700685. Superstrength through Nanotwinning. Nano Letters, 2016, 16, 7573-7579. Atomic-Level Understanding of @cœAsymmetric Twins@cin Boron Carbide. Physical Review Letters, 2015, 115, 175501. New Ground-State Crystal Structure of Elemental Boron. Physical Review Letters, 2016, 117, 085501. Enhanced grain refinement of an Al&C*Mg&c*Si aloy by high-pressure torsion processing at 100ŰC. Processing, 2012, 552, 415-418. Effect of Nb Microalloying and Hot Rolling on Microstructure and Properties of Ultrathin Cast Strip Steels Produced by the CASTRIPA® Process. Metallurgical and Materials Transactions A: Physical Metallurg and Materials Science, 2011, 42, 2199-2206. Locating Si atoms in Si-doped boron carbide: A route to understand amorphization mitigation mechanism. Acta Materiala, 2021, 207, 116691. Significant disparity of non-basal dislocation activities in hot-rolled highly-textured Mg and Mg-3AL2n alloy under tension. Acta Materiala, 2021, 207, 116691. Effect of Alumina on the Structure and Mechanical Properties of Spark Plasma Sintered Boron 	7.3	81
 deformed by twinning and slip. Acta Materialia, 2019, 181, 555-569. Bioactive mesoporeâ€glass microspheres with controllable proteinâ€delivery properties by biomimetic surface modification. Journal of Biomedical Materials Research - Part A, 2010, 95A, 476-485. Nanotwinned metal MEMS films with unprecedented strength and stability. Science Advances, 2017, 3, e1700685. Superstrength through Nanotwinning. Nano Letters, 2016, 16, 7573-7579. Atomic-Level Understanding of "Asymmetric Twinsâ€in Boron Carbide. Physical Review Letters, 2015, 115, 175501. New Ground-State Crystal Structure of Elemental Boron. Physical Review Letters, 2016, 117, 085501. Enhanced grain refinement of an Al〓Mg–Si alloy by high-pressure torsion processing at 100°C. Materials Science & amp: Engineering A: Structural Materials: Properties of Ultrathin Cast Strip Steels Produced by the CASTRIPA® Process. Metallurgical and Materials Transactions A: Physical Metallurgy and Materials Science, 2011, 42, 2199-2206. Locating Si atoms in Si-doped boron carbide: A route to understand amorphization mitigation mechanism. Acta Materialia, 2018, 157, 106-113. Significant disparity of non-basal dislocation activities in hot-rolled highly-textured Mg and Mg-3Al-12n alloy under tension. Acta Materialia, 2021, 207, 116691. Effect of Alumina on the Structure and Mechanical Properties of Spark Plasma Sintered Boron 	12.2	77
 ⁹ surface modification. Journal of Biomedical Materials Research - Part A, 2010, 95A, 476-485. ¹⁰ Nanotwinned metal MEMS films with unprecedented strength and stability. Science Advances, 2017, 3, e1700685. ¹¹ Superstrength through Nanotwinning. Nano Letters, 2016, 16, 7573-7579. ¹² Atomic-Level Understanding of "Asymmetric Twinsâ€in Boron Carbide. Physical Review Letters, 2015, 115, 175501. ¹³ New Ground-State Crystal Structure of Elemental Boron. Physical Review Letters, 2016, 117, 085501. ¹⁴ Enhanced grain refinement of an Al–Mg–Si alloy by high-pressure torsion processing at 100ŰC. ¹⁵ Enhanced grain refinement of an Al–Mg—Si alloy by high-pressure torsion processing at 100ŰC. ¹⁶ Enterna Science & amp; Engineering A: Structural Materials: Properties, Microstructure and Processing, 2012, 552, 415-418. ¹⁷ Effect of Nb Microalloying and Hot Rolling on Microstructure and Properties of Ultrathin Cast Strip Steels Produced by the CASTRIPA® Process. Metallurgical and Materials Transactions A: Physical Metallurgy and Materials Science, 2011, 42, 2199-2206. ¹⁶ Locating Si atoms in Si-doped boron carbide: A route to understand amorphization mitigation mechanism. Acta Materialia, 2018, 157, 106-113. ¹⁷ Significant disparity of non-basal dislocation activities in hot-rolled highly-textured Mg and Mg-3Al-12n alloy under tension. Acta Materialia, 2021, 207, 116691. ¹⁸ Effect of Alumina on the Structure and Mechanical Properties of Spark Plasma Sintered Boron 	7.9	72
 e1700685. Superstrength through Nanotwinning. Nano Letters, 2016, 16, 7573-7579. Atomic-Level Understanding of "Asymmetric Twins―in Boron Carbide. Physical Review Letters, 2015, 115, 175501. New Ground-State Crystal Structure of Elemental Boron. Physical Review Letters, 2016, 117, 085501. Enhanced grain refinement of an Al〓Mg〓Si alloy by high-pressure torsion processing at 100°C. Materials Science & amp; Engineering A: Structural Materials: Properties, Microstructure and Processing, 2012, 552, 415-418. Effect of Nb Microalloying and Hot Rolling on Microstructure and Properties of Ultrathin Cast Strip Steels Produced by the CASTRIPA® Process. Metallurgical and Materials Transactions A: Physical Metallurgy and Materials Science, 2011, 42, 2199-2206. Locating Si atoms in Si-doped boron carbide: A route to understand amorphization mitigation mechanism. Acta Materialia, 2018, 157, 106-113. Significant disparity of non-basal dislocation activities in hot-rolled highly-textured Mg and Mg-3A+12n alloy under tension. Acta Materialia, 2021, 207, 116691. Effect of Alumina on the Structure and Mechanical Properties of Spark Plasma Sintered Boron 	4.0	70
12 Atomic-Level Understanding of "Asymmetric Twins―in Boron Carbide. Physical Review Letters, 2015, 115, 175501. 13 New Ground-State Crystal Structure of Elemental Boron. Physical Review Letters, 2016, 117, 085501. 14 Enhanced grain refinement of an Al–Mg–Si alloy by high-pressure torsion processing at 100°C. 14 Materials Science & amp; Engineering A: Structural Materials: Properties, Microstructure and Processing, 2012, 552, 415-418. 15 Effect of Nb Microalloying and Hot Rolling on Microstructure and Properties of Ultrathin Cast Strip Steels Produced by the CASTRIPÅ® Process. Metallurgical and Materials Transactions A: Physical Metallurgy and Materials Science, 2011, 42, 2199-2206. 16 Locating Si atoms in Si-doped boron carbide: A route to understand amorphization mitigation mechanism. Acta Materialia, 2018, 157, 106-113. 17 Significant disparity of non-basal dislocation activities in hot-rolled highly-textured Mg and Mg-3Al-12n alloy under tension. Acta Materialia, 2021, 207, 116691. 18 Effect of Alumina on the Structure and Mechanical Properties of Spark Plasma Sintered Boron	10.3	68
 12 175501. 13 New Ground-State Crystal Structure of Elemental Boron. Physical Review Letters, 2016, 117, 085501. 14 Enhanced grain refinement of an Al–Mg–Si alloy by high-pressure torsion processing at 100°C. Materials Science & amp; Engineering A: Structural Materials: Properties, Microstructure and Processing, 2012, 552, 415-418. 15 Effect of Nb Microalloying and Hot Rolling on Microstructure and Properties of Ultrathin Cast Strip Steels Produced by the CASTRIPA® Process. Metallurgical and Materials Transactions A: Physical Metallurgy and Materials Science, 2011, 42, 2199-2206. 16 Locating Si atoms in Si-doped boron carbide: A route to understand amorphization mitigation mechanism. Acta Materialia, 2018, 157, 106-113. 17 Significant disparity of non-basal dislocation activities in hot-rolled highly-textured Mg and Mg-3Al-1Zn alloy under tension. Acta Materialia, 2021, 207, 116691. 18 Effect of Alumina on the Structure and Mechanical Properties of Spark Plasma Sintered Boron 	9.1	62
 Enhanced grain refinement of an Al–Mg–Si alloy by high-pressure torsion processing at 100°C. Materials Science & amp; Engineering A: Structural Materials: Properties, Microstructure and Processing, 2012, 552, 415-418. Effect of Nb Microalloying and Hot Rolling on Microstructure and Properties of Ultrathin Cast Strip Steels Produced by the CASTRIPA® Process. Metallurgical and Materials Transactions A: Physical Metallurgy and Materials Science, 2011, 42, 2199-2206. Locating Si atoms in Si-doped boron carbide: A route to understand amorphization mitigation mechanism. Acta Materialia, 2018, 157, 106-113. Significant disparity of non-basal dislocation activities in hot-rolled highly-textured Mg and Mg-3Al-12n alloy under tension. Acta Materialia, 2021, 207, 116691. Effect of Alumina on the Structure and Mechanical Properties of Spark Plasma Sintered Boron 	7.8	56
 Materials Science & Engineering A: Structural Materials: Properties, Microstructure and Processing, 2012, 552, 415-418. Effect of Nb Microalloying and Hot Rolling on Microstructure and Properties of Ultrathin Cast Strip Steels Produced by the CASTRIPA® Process. Metallurgical and Materials Transactions A: Physical Metallurgy and Materials Science, 2011, 42, 2199-2206. Locating Si atoms in Si-doped boron carbide: A route to understand amorphization mitigation mechanism. Acta Materialia, 2018, 157, 106-113. Significant disparity of non-basal dislocation activities in hot-rolled highly-textured Mg and Mg-3Al-1Zn alloy under tension. Acta Materialia, 2021, 207, 116691. Effect of Alumina on the Structure and Mechanical Properties of Spark Plasma Sintered Boron 	7.8	44
 Steels Produced by the CASTRIPA® Process. Metallurgical and Materials Transactions A: Physical Metallurgy and Materials Science, 2011, 42, 2199-2206. Locating Si atoms in Si-doped boron carbide: A route to understand amorphization mitigation mechanism. Acta Materialia, 2018, 157, 106-113. Significant disparity of non-basal dislocation activities in hot-rolled highly-textured Mg and Mg-3Al-1Zn alloy under tension. Acta Materialia, 2021, 207, 116691. Effect of Alumina on the Structure and Mechanical Properties of Spark Plasma Sintered Boron 	5.6	43
 ¹⁶ mechanism. Acta Materialia, 2018, 157, 106-113. ¹⁷ Significant disparity of non-basal dislocation activities in hot-rolled highly-textured Mg and Mg-3Al-1Zn alloy under tension. Acta Materialia, 2021, 207, 116691. ¹⁸ Effect of Alumina on the Structure and Mechanical Properties of Spark Plasma Sintered Boron 	2.2	42
 ¹⁷ Mg-3Al-1Zn alloy under tension. Acta Materialia, 2021, 207, 116691. ¹⁸ Effect of Alumina on the Structure and Mechanical Properties of Spark Plasma Sintered Boron 	7.9	42
	7.9	41
Carbide. Journal of the American Ceramic Society, 2014, 97, 3710-3718.	3.8	36

YUXUAN XIE

#	Article	IF	CITATIONS
19	Microstructural Characterization of a Commercial Hotâ€Pressed Boron Carbide Armor Plate. Journal of the American Ceramic Society, 2016, 99, 2834-2841.	3.8	36
20	Effect of crystallite geometries on electrochemical performance of porous intercalation electrodes by multiscale operando investigation. Nature Materials, 2022, 21, 217-227.	27.5	35
21	The effect of pre-existing defects on the strength and deformation behavior of α-Fe nanopillars. Acta Materialia, 2013, 61, 439-452.	7.9	33
22	Damage evolution of hot-pressed boron carbide under confined dynamic compression. International Journal of Impact Engineering, 2017, 99, 75-84.	5.0	33
23	Breaking the icosahedra in boron carbide. Proceedings of the National Academy of Sciences of the United States of America, 2016, 113, 12012-12016.	7.1	31
24	The effect of Si on the microstructure and mechanical properties of spark plasma sintered boron carbide. Materials Characterization, 2017, 134, 274-278.	4.4	31
25	Resolving the Morphology of Niobium Carbonitride Nano-Precipitates in Steel Using Atom Probe Tomography. Microscopy and Microanalysis, 2014, 20, 1100-1110.	0.4	30
26	Exploring the origins of the indentation size effect at submicron scales. Proceedings of the National Academy of Sciences of the United States of America, 2021, 118, .	7.1	29
27	Cluster strengthening of Nb-microalloyed ultra-thin cast strip steels produced by the CASTRIP® process. Materials Science & Engineering A: Structural Materials: Properties, Microstructure and Processing, 2013, 568, 88-95.	5.6	26
28	Tuning the deformation mechanisms of boron carbide via silicon doping. Science Advances, 2019, 5, eaay0352.	10.3	26
29	A facile method to in situ formation of hydroxyapatite single crystal architecture for enhanced osteoblast adhesion. Journal of Materials Chemistry, 2012, 22, 19081.	6.7	25
30	Activation and suppression of ã€^cÂ+Âa〉 dislocations in a textured Mg–3Al–1Zn alloy. Scripta Materialia, 2020, 179, 49-54.	5.2	22
31	The effect of clustering on the mobility of dislocations during aging in Nb-microalloyed strip cast steels: In situ heating TEM observations. Scripta Materialia, 2013, 69, 481-484.	5.2	21
32	Effect of temperature on the transition in deformation modes in Mg single crystals. Acta Materialia, 2019, 178, 241-248.	7.9	21
33	Insight into the deformation mechanisms of α-Fe at the nanoscale. Scripta Materialia, 2011, 65, 1037-1040.	5.2	20
34	Understanding of Lithium Insertion into 3D Porous Carbon Scaffolds with Hybridized Lithiophobic and Lithiophilic Surfaces by In-Operando Study. Nano Letters, 2020, 20, 3681-3687.	9.1	20
35	Ultrahigh-strength submicron-sized metallic glass wires. Scripta Materialia, 2014, 84-85, 27-30.	5.2	17
36	Fabrication of dense B4C-preceramic polymer derived SiC composite. Journal of the European Ceramic Society, 2019, 39, 718-725.	5.7	17

YUXUAN XIE

#	Article	IF	CITATIONS
37	Overcoming challenges in the study of nitrided microalloyed steels using atom probe. Ultramicroscopy, 2012, 112, 32-38.	1.9	15
38	Understanding the interaction of extension twinning and basal-plate precipitates in Mg-9Al using precession electron diffraction. Materialia, 2021, 15, 101044.	2.7	15
39	Experimental observations of the mechanisms associated with the high hardening and low strain to failure of magnesium. Materialia, 2019, 8, 100504.	2.7	13
40	Grain-subdivision-dominated microstructure evolution in shear bands at high rates. Materials Research Letters, 2020, 8, 328-334.	8.7	13
41	In vitro study of the effect of cyclic strains on the dermal fibroblast (GM3384) morphology—Mapping of cell responses to strain field. Medical Engineering and Physics, 2012, 34, 826-831.	1.7	12
42	Precipitation of AlN in a commercial hot-pressed boron carbide. Scripta Materialia, 2015, 101, 95-98.	5.2	12
43	An etÂal. Reply:. Physical Review Letters, 2017, 118, 089602.	7.8	12
44	Small amount TiB ₂ addition into B ₄ C through sputter deposition and hot pressing. Journal of the American Ceramic Society, 2019, 102, 4421-4426.	3.8	12
45	Molten salt synthesis of highly ordered and nanostructured hexagonal boron nitride. Diamond and Related Materials, 2019, 93, 179-186.	3.9	12
46	Twin boundary migration mechanisms in quasi-statically compressed and plate-impacted Mg single crystals. Science Advances, 2021, 7, eabg3443.	10.3	12
47	Twinning pathways enabled by precipitates in AZ91. Materialia, 2022, 21, 101292.	2.7	12
48	Addressing amorphization and transgranular fracture of B ₄ C through Si doping and TiB ₂ microparticle reinforcing. Journal of the American Ceramic Society, 2022, 105, 2959-2977.	3.8	11
49	High Moisture Barrier with Synergistic Combination of SiO <i>_x</i> and Polyelectrolyte Nanolayers. Advanced Materials Interfaces, 2019, 6, 1900740.	3.7	10
50	Effect of synthesis conditions of BCNO on the formation and structural ordering of boron nitride at high temperatures. Journal of Solid State Chemistry, 2019, 269, 212-219.	2.9	10
51	Formation of metastable wurtzite phase boron nitride by emulsion detonation synthesis. Journal of the American Ceramic Society, 2018, 101, 3276-3281.	3.8	9
52	Non-dissociated <c+a> dislocations in an AZ31 alloy revealed by transmission electron microscopy. Materials Research Letters, 2020, 8, 145-150.</c+a>	8.7	8
53	Nano-scale Elastic Strain Maps of Twins in Magnesium Alloys. Microscopy and Microanalysis, 2018, 24, 970-971.	0.4	7
54	On the exceptionally high ductility of Mg–2Zn-0.3Ca-0.2Ce-0.1Mn alloy. Materials Science & Engineering A: Structural Materials: Properties, Microstructure and Processing, 2021, 819, 141484.	5.6	6

Yuxuan Xie

#	Article	IF	CITATIONS
55	Large areal capacity and dendrite-free anodes with long lifetime enabled by distributed lithium plating with mossy manganese oxides. Journal of Materials Chemistry A, 2021, 9, 9291-9300.	10.3	6
56	Effect of local twin Schmid factor on the tension twinning activities in a highly textured Mg–3Al–1Zn alloy under different strain paths. MRS Communications, 2022, 12, 217-222.	1.8	6
57	Decoupling the metal–insulator transition temperature and hysteresis of VO ₂ using Ge alloying and oxygen vacancies. Chemical Communications, 2022, 58, 6586-6589.	4.1	6
58	Spatial decomposition of molecular ions within 3D atom probe reconstructions. Ultramicroscopy, 2013, 132, 92-99.	1.9	5
59	The Effect of Microstructure Morphology on Indentation Response of Ta/Ti Nanocomposite Thin Films. Metallurgical and Materials Transactions A: Physical Metallurgy and Materials Science, 2020, 51, 5677-5690.	2.2	5
60	The mechanical behaviour of TiN and multi-layered coating of TiN/Ti on Ti6Al4V substrate during nano-indentation. International Journal of Surface Science and Engineering, 2014, 8, 95.	0.4	4
61	Persistence of crystal orientations across sub-micron-scale "super-grains―in self-organized Cu-W nanocomposites. Scripta Materialia, 2021, 194, 113677.	5.2	4
62	Experimental observations of amorphization in multiple generations of boron carbide. Journal of the American Ceramic Society, 2022, 105, 3008-3029.	3.8	4
63	Structure and substructure characterization of solution-treated Ni50.3Ti29.7Hf20 high-temperature shape memory alloy. Scripta Materialia, 2022, 219, 114888.	5.2	4
64	High Strength and Retained Ductility Achieved in a Nitrided Strip Cast Nb-Microalloyed Steel. Metallurgical and Materials Transactions A: Physical Metallurgy and Materials Science, 2013, 44, 848-855.	2.2	3
65	Interface stability of laser powder-bed-fused AlSi12 under simulated atmospheric conditions. Corrosion Science, 2020, 175, 108861.	6.6	3
66	The effect of boron and aluminum additions on the microstructure of arcâ€melted boron carbide. Journal of the American Ceramic Society, 2020, 103, 3453-3457.	3.8	3
67	Nitriding of a Nb-Microalloyed Thin Strip Cast Steel at 525°C. Materials Science Forum, 0, 654-656, 106-109.	0.3	2
68	An Overview of the Effect of Nb in Strengthening Castrip [®] Steel. Materials Science Forum, 2013, 753, 559-562.	0.3	2
69	The mechanical behavior of single crystal and polycrystalline pure magnesium. Mechanics of Materials, 2021, 163, 104078.	3.2	2
70	Damage relief of ion-irradiated Inconel alloy 718 via annealing. Nuclear Instruments & Methods in Physics Research B, 2020, 479, 157-162.	1.4	2
71	Revealing the Microstructural Information of the Quasi-Plastic Zone in a Boron Carbide Using the Advanced Precession Electron Diffraction Technique. Microscopy and Microanalysis, 2019, 25, 788-789.	0.4	1
72	Dislocation Imaging by Precession Electron Diffraction. Microscopy and Microanalysis, 2020, 26, 226-227.	0.4	1

YUXUAN XIE

#	Article	IF	CITATIONS
73	Comparative study of helium bubbles in a Ti-Ta alloy and a Ti/Ta nanocomposite. Philosophical Magazine Letters, 2020, 100, 307-318.	1.2	1
74	In vitro studies of cells grown on the superconductor PrOxFeAs. Micron, 2009, 40, 476-479.	2.2	0
75	Effect of Twin Schmid Factor on the Tension Twinning Activities in a Highly Textured Mg-3Al-1Zn. SSRN Electronic Journal, 0, , .	0.4	0
76	Dislocation imaging via the virtual dark-field technique using the precession electron diffraction data. Microscopy and Microanalysis, 2021, 27, 2916-2917.	0.4	0
77	Applications of analytical electron microscopy to guide the design of boron carbide. Journal of the American Ceramic Society, 0, , .	3.8	0
78	Deformation behavior of Mg single crystals compressed along c-axis. , 2016, , 209-211.		0